ResearchGate

See discussions, stats, and author profiles for this publication at: https://www.researchgate.net/publication/228922096

One-Pot Template-Free Fabrication of Hollow Magnetite Nanospheres and Their Application as Potential Drug Carriers

ARTICLE *in* THE JOURNAL OF PHYSICAL CHEMISTRY C · DECEMBER 2009

Impact Factor: 4.77 · DOI: 10.1021/jp907296n

CITATIONS
80

READS
132

5 AUTHORS, INCLUDING:

Shanhu Liu
Henan University
34 PUBLICATIONS **457** CITATIONS
SEE PROFILE

Ruimin Xing
Henan University
21 PUBLICATIONS **424** CITATIONS
SEE PROFILE

Available from: Shanhu Liu
Retrieved on: 26 January 2016

One-Pot Template-Free Fabrication of Hollow Magnetite Nanospheres and Their Application as Potential Drug Carriers

Shanhu Liu,[†] Ruimin Xing,[†] Feng Lu,[†] Rohit Kumar Rana,[‡] and Jun-Jie Zhu*,[†]

Key Laboratory of Analytical Chemistry for Life Science, Ministry of Education of China, School of Chemistry and Chemical Engineering, Nanjing University, Nanjing 210093, People's Republic of China, and Nanomaterials Laboratory, Inorganic and Physical Chemistry Division, Indian Institute of Chemical Technology, Hyderabad 500 607, India

Received: July 30, 2009; Revised Manuscript Received: October 26, 2009

Monodispersed Fe_3O_4 nanospheres with hollow interior structures exhibiting high saturation magnetization of 83.0 emu g^{-1} were fabricated by a facile one-pot route. The fabrication process is very simple with only $FeCl_3 \cdot 6H_2O$ and anhydrous NaAc as the reactants in an ethylene glycol solution with no templates or surfactants involved. Field-emission scanning electron microscopy, transmission electron microscopy, X-ray photoelectron spectroscopy, and a superconducting quantum interference device magnetometer were used to characterize the morphologies, structures, and properties of the hollow magnetic nanospheres. A plausible mechanism based on oriented attachment and subsequent local Ostwald ripening is proposed. In addition, the experiments of the hollow nanospheres decorated with polyacrylic acids as drug carriers and Rhodamine 6G as a model drug, revealed pH- or salt-responsive release profiles, thus demonstrating the potential of these nanostructures in biomedical applications.

Introduction

The reliance of future technologies on exploring facile and economic methods for the fabrication of magnetic materials has spurred intense and rapid development in the field of materials science.[1−3] In particular, iron oxide-based magnetic materials have been extensively pursued for multidisciplinary researches, not only for fundamental size-dependent magnetism[4] and optoelectronics[5] but also for biomedical applications due to their low toxicity.[6−8] Various methods such as coprecipitation,[9] hydrothermal reaction,[10,11] microemulsion synthesis, and thermal decomposition and/or reduction techniques[3,12,13] have been directed in the synthesis of iron oxide nanoparticles.[14] However, much attention has been focused on the size, protection, and functionalization of magnetic nanopoarticles;[2,15] effective methods for the fabrication of interesting magnetic structures and their shape regulation remain underdeveloped. Among them, iron oxide-based magnetic structures with an interior void could integrate the benefits of hollow structures and magnetic properties. They are of great interest due to their large surface area and low material density as well as strong magnetic response. The magnetic hollow nanostructures are envisaged to serve as hosts for encapsulating guest molecules and sensitive materials such as drugs, proteins cosmetics, and catalysts; and they could be manipulated by an external magnetic field.[16−18] Recently, several strategies for synthesizing hollow structures such as the nanoscale Kirkendall effect,[16] Ostwald ripening,[19] molten salt corrosion,[17] reverse micelle transport,[20] and layer-by-layer assembly[21,22] have been attempted. These fabrication approaches are conventionally based on the well-established template methods,[23] such as hard-template,[22,24] soft-template,[10,20,25,26] and sacrificial template.[16] Template methods have proven to be effective and versatile for the synthesis of a wide array of hollow structures. Nonetheless, disadvantages related to tedious synthetic procedures and low yields have impeded the scale-up production and large-scale applications. Therefore, to develop a facile and efficient route becomes the major aims for the fabrication of magnetic hollow structures. In a sense, one-pot template-free synthesis is desirable and preferred.

Herein, we report a one-pot hydrothermal method to fabricate hollow magnetite nanospheres (HMNs) without use of any templates or surfactants. Inexpensive and nontoxic reagents such as $FeCl_3 \cdot 6H_2O$ and anhydrous NaAc were used in the ethylene glycol (EG) solution. Microstructural analyses and properties evaluation revealed that the product was flowerlike magnetite nanospheres with hollow interior structures and these nanospheres were made up of smaller building blocks of magnetite nanoparticles. The HMNs exhibited high saturation magnetization with a ferromagnetic behavior. A plausible mechanism is proposed for the hollow structure formation. In addition, the application of HMNs as drug carriers is demonstrated by using Rhodamine 6G (R6G) as a model drug.

Experimental Section

Chemicals. Poly acrylic acid (PAA, 35% w/w in water, MW=100,000) and R6G were purchased from Sigma-Aldrich Chemical Reagent Co., Ltd. $FeCl_3 \cdot 6H_2O$, anhydrous NaAc, EG, and other chemical reagents were of analytical grade and used as received without further purification. Phosphate buffered saline (PBS, 0.01 M, pH 7.4) and acetate buffer saline (0.01 M, pH 3.7) solutions were prepared according to the documented procedures. Millipore water (18.2 MΩ cm at 25 °C) was used throughout all experiments.

Preparation of Hollow Magnetite Nanospheres. HMNs were fabricated by hydrothermal treatment of $FeCl_3 \cdot 6H_2O$ and NaAc in the EG solution. In a typical procedure, 20 mmol of $FeCl_3 \cdot 6H_2O$ was dissolved in 40 mL of EG to form a clear solution, followed by the addition of 40 mmoL of anhydrous

* To whom correspondence should be addressed. Tel.: +86 25 83594976. Fax: +86 25 83594976. E-mail: jjzhu@nju.edu.cn.
[†] Nanjing University.
[‡] Indian Institute of Chemical Technology.

10.1021/jp907296n CCC: $40.75 © 2009 American Chemical Society
Published on Web 11/19/2009

NaAc. The mixture was vigorously mixed by ultrasonication to give a homogeneous solution. Then the solution was transferred into a Teflon-lined stainless steel autoclave (50 mL capacity) for hydrothermal treatment at 200 °C for 10 h. After the autoclave was allowed to cool down to room temperature, the precipitate was collected by magnetic separation and washed several times under sonication with water and ethanol and then dried under vacuum at room temperature before characterization and application.

To investigate the influence of $FeCl_3 \cdot 6H_2O$ and reaction time on the morphology of Fe_3O_4 nanostructures, three sets of control experiments were carried out as follows. Control A was to vary the initial amount of $FeCl_3 \cdot 6H_2O$ in the reaction, control B was to use anhydrous $FeCl_3$ instead of hexahydrate $FeCl_3$ without/with additional water, and control C was to vary the hydrothermal treatment duration. The rest of the synthesis conditions in each of these control experiments were kept the same as those in the typical experiment described above.

Drug Loading and Release. The drug loading and in vitro release profiles were obtained by the reported methods.[27−31] First, 10 mg of HMNs were dispersed in an aqueous solution of PAA (0.25% in 0.5 M NaCl) and were sonicated for 20 min to give a suspension. Redundant PAA polymer was removed by magnetic separation and the as-prepared carboxylated HMNs were washed with water for at least three times and denoted hereafter as PAA-HMNs. To load R6G on PAA-HMNs, 2 μg/mL of R6G solution was incubated with increasing amounts of PAA-HMNs (2, 40, 80, 200, 250, 400, 600, 650, and 700 μg) for 1 h under stirring. Then, to monitor the fluorescence changes of R6G after it was loaded on PAA-HMNs, the fluorescence spectra of R6G were recorded at excitation and emission wavelengths of 350 nm and 480−680 nm, respectively. PAA-HMNs loaded with R6G were denoted hereafter as R6G@PAA-HMNs. The release profiles of R6G from R6G@PAA-HMNs were obtained as follows. R6G@PAA-HMNs were immersed in 20 mL of PBS solution (pH 7.4) or acetate buffer (pH 3.7) or pure water at 37 °C with gentle shaking, respectively. Certain amount of solutions were taken out at given time intervals and replaced with the same volume of their fresh solutions. The amount of released R6G was determined by fluorescence analysis with excitation and emission wavelengths of 350 and 552 nm, respectively.

Characterization. Field emission scanning electron microscopy (FE-SEM) images were obtained using a Hitachi S-4800 field emission electron microscope at an accelerating voltage of 5 kV. Transmission electron microscopy (TEM) images and selected area electron diffraction (SAED) patterns were taken using a JEOL JEM-2010 transmission electron microscope at an accelerating voltage of 200 kV. X-ray powder diffraction (XRD) measurements were performed on a Japan Shimadzu XRD-6000 Diffractometer with Cu Kα radiation ($\lambda = 0.15418$ nm); a scanning rate of 0.05 deg/s was applied to record the patterns in the 2θ range of 20−70°. X-ray photoelectron spectra (XPS) were obtained using a Thermo ESCALAB 250 electron spectrometer with 150 W monochromatized Al Kα radiations (1486.6 eV). The binding energy of C1s level from contamination of saturated hydrocarbons at 284.8 eV was used as internal reference to calibrate the spectra. Superconducting quantum interference device (SQUID, Quantum Design) magnetometer was used in the magnetic measurement at 300 K. Zeta potential (ζ) of HMNs and PAA-HMNs was measured in pure water on a Malven Nano-Z instrument. Fluorescence spectra were obtained on an AMINCO Bowman Series 2 instrument.

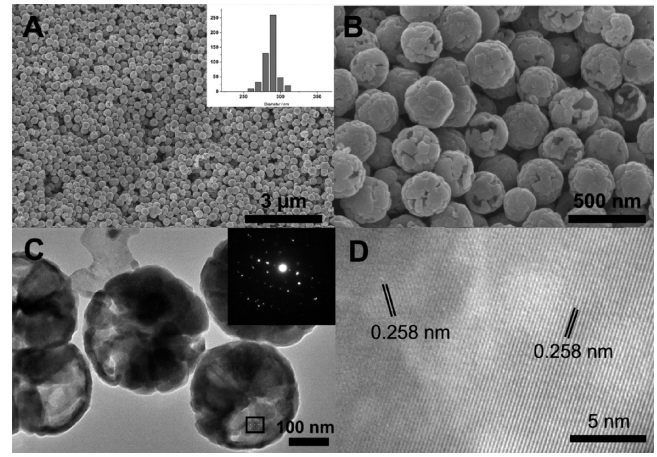

Figure 1. (A) Low-resolution SEM (insert in A shows the size distribution analysis), (B) high-resolution SEM, (C) TEM image of the hollow magnetite nanospheres obtained in the typical experiment described in the experimental section (insert in C is the SAED patterns), and (D) HRTEM image of the boxed region shown in image C.

Results and Discussion

Characterization of the As-Prepared Hollow Magnetite Nanospheres. As mentioned in the experimental section, HMNs were fabricated by a facile template-free hydrothermal route using $FeCl_3 \cdot 6H_2O$ and NaAc as raw materials in the EG solution. The morphology and size of thus obtained HMNs were investigated by SEM and TEM analyses. Parts A and B of Figure 1 are representative SEM images of HMNs. As seen in part A of Figure 1, the nanospheres are monodisperse and uniform on a large scale. A statistical analysis yields an average size of 290 nm in diameter with a size distribution standard deviation of 30 nm (insert in part A of Figure 1). Shown in part B of Figure 1 is an enlarged SEM image. It exhibits a kind of hierarchical structure of the nanospheres, which consists of smaller building blocks (ca. 50 nm) assembled together to form the shell wall. Partly bowl-shaped broken spheres with open pores prove their hollow interior structure. Compared with other hollow structures with an uniform shell wall, the nonsealed, porous nature of the above hollow nanospheres can facilitate immobilization and subsequent encapsulation of various guest molecules in a similar way as reported by Caruso et al.[32] The distinct contrast derived from the difference of electron density in the TEM image (part C of Figure 1) also confirms the hollow and hierarchical structure of the nanospheres.[33] The SAED pattern recorded on a single isolated nanosphere reveals the crystalline nature of the material (insert in part C of Figure 1). More evidence on crystallinity was obtained from the HRTEM analysis of the marked region shown in part C of Figure 1. The crystal lattice fringes seen in part D of Figure 1 indicates that the nanospheres are formed by geometrically random but lattice-oriented attachment of most of the primary particles.[34] The measured d spacing is 0.258 nm, which is in good agreement with the values for (311) planes of a cubic magnetite phase. The HRTEM observations also ascertain that the primary particles have high crystallinity and they serve as building blocks for the formation of nanospheres.

The crystal structures of these hollow nanospheres were studied by XRD analyses. As shown in part A of Figure 2, all diffraction peaks and positions matches well with those from the JCPDS card (No. 75−0033) for a cubic magnetite and well-resolved diffraction peaks reveal good crystallinity of these nanospheres. Calculations using the Debye−Scherrer formula for the strongest peak (311) showed grain sizes of 53 nm. This

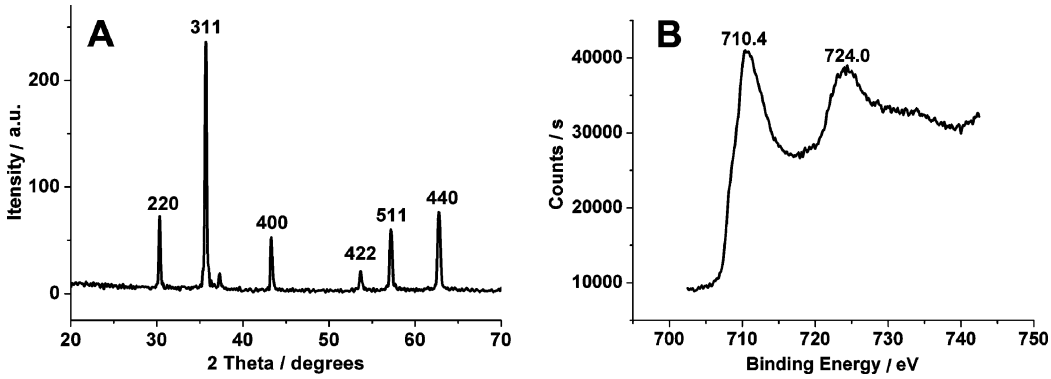

Figure 2. (A) XRD patterns and (B) Fe2p high-resolution XPS spectra of hollow magnetite nanospheres.

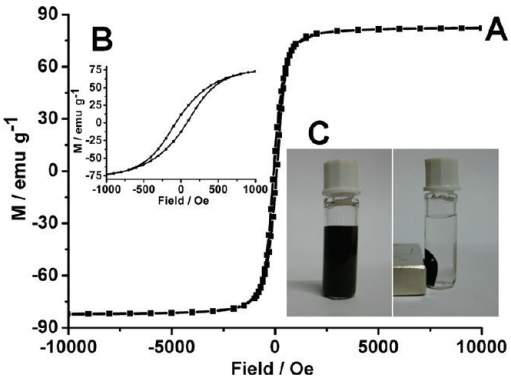

Figure 3. (A) Room-temperature magnetization curve as a function of field for HMNs, (B) enlarged curve around zero field with a scale ranging from −1000 to 1000 Oe, and (C) the photograph of the suspension of these nanospheres dispersed in water (left) and drawn from the solution to the sidewall of the vial by an external magnet (right).

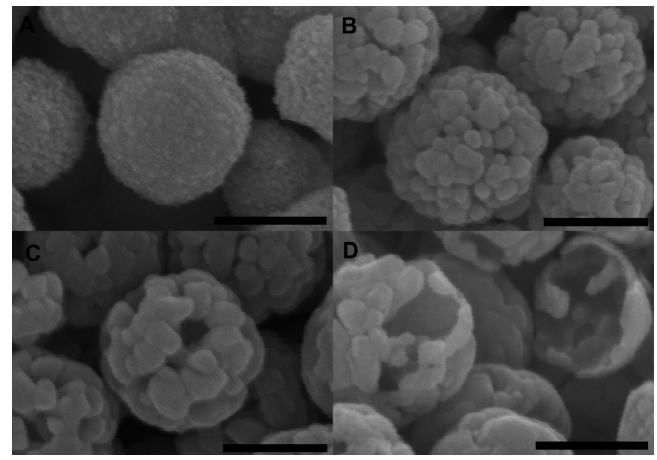

Figure 4. SEM images of the nanospheres prepared at various initial amounts of $FeCl_3 \cdot 6H_2O$: (A) 0.4 mmol, (B) 5 mmol, (C) 10 mmol, and (D) 20 mmol. All of the scale bars are 200 nm.

result further confirms the fact that the hollow nanospheres of 290 nm in size are made up of smaller building blocks of nanoparticles, which is consistent with that determined by TEM. As magnetite (Fe_3O_4) and maghemite (γ-Fe_2O_3) have similar XRD patterns and both of them exhibit magnetic behavior, the composition of the products could be further identified by XPS spectroscopy. The Fe 2p high-resolution XPS spectra (part B of Figure 2) reveal that Fe 2p has BE values of 710.4 and 724.0 eV for $2p_{3/2}$ and $2p_{1/2}$, respectively. These values are close to that the report for Fe_3O_4. Furthermore, the absence of charge transfer satellite near the photoelectron peak of $Fe2p_{3/2}$ also gives information about the mixed oxidation state of iron such as Fe_3O_4.[35]

The magnetic properties of HMNs were studied using a commercial SQUID magnetometer at room temperature. Part A of Figure 3 presents the magnetization of HMNs at 300 K by cycling the field between −10 kOe and 10 kOe. It reveals a weak ferromagnetism behavior for the HMNs with a typical hysteresis loop having a remanence of 11 emu g^{-1} and a coercivity of 75 Oe (part B of Figure 3). The saturation magnetization of the nanospheres at 300 K is 83.0 emu g^{-1}, much larger than that reported before for similar structures,[25] which implies that these nanospheres would have stronger response to an external magnet. Part C of Figure 3 shows the photographs of the suspension of HMNs in the absence and the presence of an external magnet. The nanospheres can be easily dispersed in water to form a black suspension and be drawn from the solution to the sidewall of the vial by an external magnetic field. The magnetic particles can be brought again back into the original solution by removing the external field and then slightly agitating.

Possible Formation Mechanism of Hollow Magnetite Nanospheres. In the process of hydrothermal synthesis, it is usually supposed that EG acts both as a high-boiling-point solvent and a reducing agent, whereas sodium acetate provides a basic medium. Fe(III) could partly be reduced to Fe(II) by EG. The respective ions are then hydrolyzed to form $Fe(OH)_3$ and $Fe(OH)_2$ in the basic medium, followed by the generation of Fe_3O_4 primary nanoparticles via dehydration of these hydroxides.[2,36] Afterward, the formation of Fe_3O_4 flowerlike nanospheres seemed to be reasonable through the oriented attachment of these primary particles to achieve minimization of their surface energy as well as their magnetic dipole alignment. However, further understanding is still required to know how these nanospheres transform into the hollow structures without the use of any templates.

The reaction conditions were systematically studied to further investigate the formation mechanism of HMNs. First, the influence of the initial concentration of $FeCl_3 \cdot 6H_2O$ on the morphology of the products were investigated by SEM. When the iron amount was 0.4 mmol, lots of nanospheres were formed by compact stacking of primary particles of less than 10 nm in diameter (part A of Figure 4). With increasing the amount to 5 mmol, the size of the primary particles increased with simultaneous appearance of some gaps on the flowerlike nanospheres (part B of Figure 4). When the amount increased to 10 mmol, the gaps were broadened with a clear appearance of a porous structure (part C of Figure 4). Interestingly, the hollow nanospheres eventually emerged with the iron amount of 20 mmol (part D of Figure 4). In addition, the XRD patterns indicated that all of the products

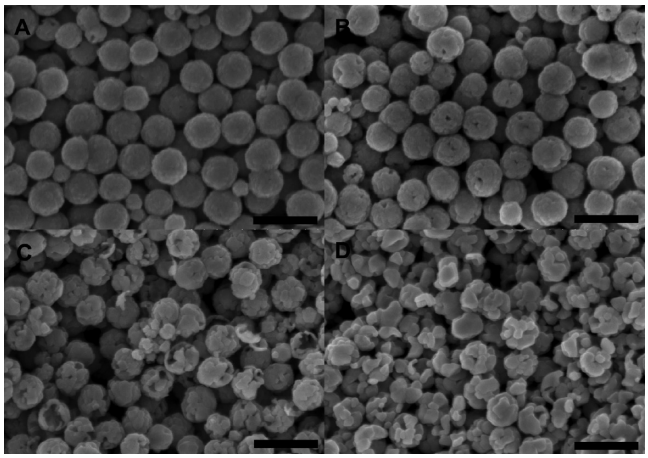

Figure 5. SEM images of the nanospheres obtained for different reaction times: (A) 5 h, (B) 6 h, (C) 10 h, and (D) 16 h. All of the scale bars are 500 nm.

are pure cubic phase of Fe_3O_4 but the nanospheres obtained with the iron amount of 0.4 mmol exhibited broader diffraction peaks than the other nanospheres obtained with higher iron amounts (Figure S1 of the Supporting Information). The XRD results are consistent with the SEM observations that the initial concentration of $FeCl_3 \cdot 6H_2O$ has a dramatic effect on the morphology and structure of the products.

The time-dependent shape evolution of Fe_3O_4 nanospheres was also studied. In a control experiment, when the reaction temperature was below 180 °C or the reaction time was less than 4 h, instead of a black product, a thick yellow mixture was formed. Figure 5 presents the typical morphology of the nanospheres for different hydrothermal treatment times. After 5 h of hydrothermal treatment, the obtained sample was composed of uniform and compact nanospheres formed by the aggregation of primary particles (part A of Figure 5). For a heating time of 6 h, some small holes on the nanospheres could be clearly observed (part B of Figure 5), which implied the appearance of hollow structures of the nanospheres. When the heating time was further increased to 10 h, the holes became larger and the interior voids became visible (part C of Figure 5). If the heating time was prolonged to 16 h, most of the nanospheres were broken or collapsed and turned into the cracked structures (part D of Figure 5). The corresponding XRD patterns could be indexed to a cubic phase of Fe_3O_4 (Figure S2 of the Supporting Information).

On the basis of all of the above observations, a plausible mechanism involving an oriented attachment followed by local Ostwald ripening is proposed to address the template-free formation of the hollow structure of HMNs.[23,34,37] In the initial reaction period, acetate groups might coordinate with iron to form the precursors of iron acetate (such as ferric acetate or ferrous acetate) because iron has a strong tendency to coordinate with carboxylate groups.[38] As the temperature increased, hydrolysis and alcoholysis were regarded as possible pathways[39] and the main reactions were speculated as follows.

$$\mathrm{Fe(Ac)}_n + \mathrm{H_2O} \overset{\Delta}{\rightleftharpoons} \mathrm{Fe_3O_4} + \mathrm{HAc}\uparrow \quad (1)$$

$$\mathrm{Fe(Ac)}_n + \mathrm{ROH} \overset{\Delta}{\longrightarrow} \mathrm{Fe_3O_4} + \mathrm{CH_3COOR} \quad (2)$$

The Fe_3O_4 primary particles are thus generated through either/or both hydrolysis and alcoholysis. As mentioned above, the flowerlike nanospheres are then formed through oriented attachment of these primary particles to minimize the surface energy of the total system. At a certain ratio of iron to acetate ligands, the different chelation modes between the outer and interior particles in the nanospheres might provide the opportunity for local ripening. On the other hand, the water derived from hexahydrate $FeCl_3$ might facilitate the process because the primary particles formed through hydrolysis are believed to be thermodynamically unstable.[39] As the reaction proceeds, the particles can be subjected to Ostwald ripening, which gradually dissolves and transforms into these stable species. In other words, further reduction in the overall surface energies provides the driving force for intraparticles ripening within the system.[40] As a result, the hollow structures of HMNs with larger building blocks were formed. To test the above hypothesis and the importance of water, anhydrous $FeCl_3$ was used as an iron source instead of hexahydrate $FeCl_3$ and three additional experiments were performed. One was to use a small amount of anhydrous $FeCl_3$ (such as 5 mmol), which did not result in any hollow structure (part A of Figure S3 of the Supporting Information). When the amount of anhydrous $FeCl_3$ increased to 20 mmol, some nanospheres with hollow structure were formed (part B of Figure S3 of the Supporting Information). Interestingly, addition of water brought more hollow structures (part C of

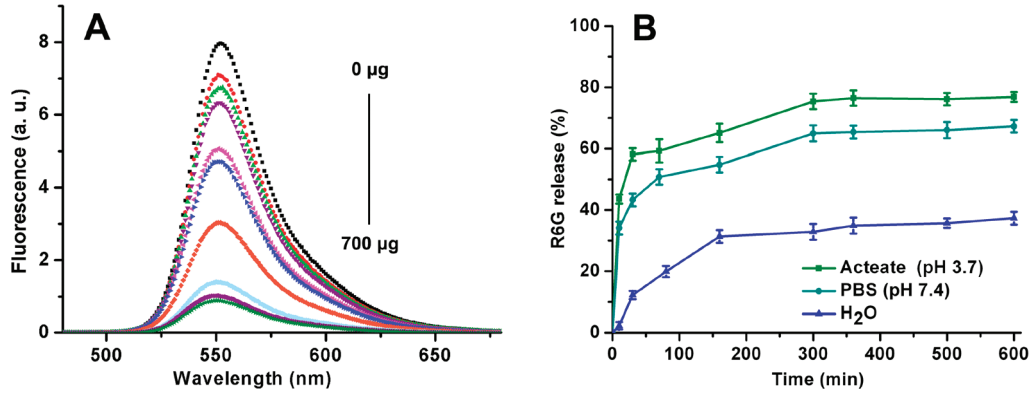

Figure 6. (A) Fluorescence spectra of R6G solution (8 μg in 4 mL of water) with increasing amounts of PAA-HMNs (from top to bottom: 0, 2, 40, 80, 200, 250, 400, 600, 650, 700 μg) with the excitation wavelength of 350 nm; (B) R6G release profiles for R6G@PAA-HMNs measured in acetate buffer (pH 3.7) and in PBS (pH 7.4) as well as pure water solution.

Figure S3 of the Supporting Information). These results clearly support the above proposed mechanism.

Application of Hollow Magnetite Nanospheres as Potential Drug Carriers. To investigate the potential application of HMNs as drug carriers, drug loading, and in vitro release studies were carried out as follows. First, PAA-HMNs were fabricated by anchoring PAA on the external and internal surfaces of HMNs via the self-assembly method. Redundant PAA was efficiently removed by magnetic separation and washing. The charge reversal in the zeta potential of PAA-HMNs (-39.5 ± 0.8 mV) relative to that of HMNs ($+6.8 \pm 0.6$ mV) clearly implied that HMNs were modified with negatively charged carboxylate groups. R6G was chosen as model drugs because it is a cationic dye that can bind with negatively charged carboxylate groups. In the loading process, the formation of R6G containing PAA-HMNs (R6G@PAA-HMNs) was accompanied with a simultaneous quenching of R6G fluorescence as a result of R6G binding with PAA-HMNs via electrostatic interaction.[27,31] A sequential decrease in the fluorescence intensity of R6G was observed with increasing amounts of PAA-HMNs. The maximal quenching of R6G fluorescence was observed with approximately 8 μg of R6G to 700 μg of PAA-HMNs, indicative of the optimal loading of R6G to PAA-HMNs (part A of Figure 6). The in vitro drug-release kinetics of R6G@PAA-HMNs was studied against two buffer solutions as well as pure water system at 37 °C. As shown in part B of Figure 6, the release rates of R6G from the three systems were different. For the pure water system, the release rate was very slow and the released amount never exceeded about 30% of the total amount. The half-lives of R6G released at pH 7.4 in PBS and at pH 3.7 in acetate buffer were determined to be about 80 and 40 min, respectively. The salt and acidic effect could weaken the binding between R6G and carboxylate groups of PAA-HMNs.[27,41] Thus, the two buffer solutions resulted in the enhanced R6G release compared to the pure water solution as a consequence of the salt effect (ca. 0.1 mol/L NaCl) of the buffer solutions; and R6G release was faster at low pH than at neutral pH, resulting from more protonated carboxylate groups in the acetate buffer solution than in the PBS solution. In the control experiment (R6G was loaded on the HMNs without PAA modification), the release amount of R6G from R6G@HMNs was examined by PL with the same conditions. There is a negligible emission detected, indicating that a small amount of R6G was loaded on the HMNs. Therefore, the pH- or salt-responsive release profiles could be achieved by coating PAA on HMNs in the different solutions with varied pH conditions or salt concentrations.

Conclusions

In summary, a facile one-pot template-free hydrothermal route has been developed to fabricate flowerlike Fe_3O_4 nanospheres with hollow interior structures. All of the reactants are common reagents and they are inexpensive and nontoxic. Microstructural analysis and properties evaluation of the product revealed that the HMNs exhibit a kind of hierarchical structure consisting of many building blocks of smaller magnetite nanoparticles. The HMNs are monodisperse in size with a porous shell wall, especially suitable for encapsulation and release of guest molecules. The HMNs are ferromagnetic in nature with a high saturation magnetization of 83.0 emu g^{-1} at 300 K. Investigation of the formation mechanism showed that the initial amounts of $FeCl_3 \cdot 6H_2O$ played a key role in the hollow structure formation; furthermore, a plausible mechanism based on oriented attachment and subsequent local Ostwald ripening was proposed. In addition, the potential application of HMNs as a drug carrier was evaluated with R6G as a model drug, which showed a pH- or salt-dependent release profile. In addition, the demonstrated environmentally benign approach could be extended to the creation of other inorganic complex structures, which would find widespread technological and biological applications.

Acknowledgment. We greatly appreciate the support of the National Natural Science Foundation of China (20635020, 20821063), the Project of Environmental Protection Department from Jiangsu Province, China (2008003) and the Scientific Research Foundation of Graduate School of Nanjing University. This work is also supported by National Basic Research Program of China (2006CB933201).

Supporting Information Available: XRD patterns and SEM images of the products synthesized under different experiment conditions. This material is available free of charge via the Internet at http://pubs.acs.org.

References and Notes

(1) Deng, H.; Li, X. L.; Peng, Q.; Wang, X.; Chen, J. P.; Li, Y. D. *Angew. Chem., Int. Ed.* **2005**, *44*, 2782.
(2) Lu, A. H.; Salabas, E. L.; Schuth, F. *Angew. Chem., Int. Ed.* **2007**, *46*, 1222.
(3) Park, J.; An, K.; Hwang, Y.; Park, J.-G.; Noh, H.-J.; Kim, J.-Y.; Park, J.-H.; Hwang, N.-M.; Hyeon, T. *Nat. Mater.* **2004**, *3*, 891.
(4) Ge, J. P.; Hu, Y. X.; Biasini, M.; Beyermann, W. P.; Yin, Y. D. *Angew. Chem., Int. Ed.* **2007**, *46*, 4342.
(5) Ge, J. P.; Hu, Y. X.; Yin, Y. D. *Angew. Chem., Int. Ed.* **2007**, *46*, 7428.
(6) Nam, J.-M.; Thaxton, C. S.; Mirkin, C. A. *Science* **2003**, *301*, 1884.
(7) Gao, L.; Wu, J.; Lyle, S.; Zehr, K.; Cao, L.; Gao, D. *J. Phys. Chem. C* **2008**, *112*, 17357.
(8) Gao, L. Z.; Zhuang, J.; Nie, L.; Zhang, J. B.; Zhang, Y.; Gu, N.; Wang, T. H.; Feng, J.; Yang, D. L.; Perrett, S.; Yan, X. *Nat. Nanotechnol.* **2007**, *2*, 577.
(9) Fried, T.; Shemer, G.; Markovich, G. *Adv. Mater.* **2001**, *13*, 1158.
(10) Wang, L.; Bao, J.; Wang, L.; Zhang, F.; Li, Y. D. *Chem.—Eur. J.* **2006**, *12*, 6341.
(11) Arruebo, M.; Fernandez-Pacheco, R.; Ibarra, M. R.; Santamaria, J. *Nano Today* **2007**, *2*, 22.
(12) Sun, S.; Zeng, H.; Robinson, D. B.; Raoux, S.; Rice, P. M.; Wang, S. X.; Li, G. *J. Am. Chem. Soc.* **2004**, *126*, 273.
(13) Lee, Y.; Lee, J.; Bae, C. J.; Park, J. G.; Noh, H. J.; Park, J. H.; Hyeon, T. *Adv. Funct. Mater.* **2005**, *15*, 503.
(14) Wang, X.; Zhuang, J.; Peng, Q.; Li, Y. D. *Nature* **2005**, *437*, 121.
(15) Wang, L.; Yang, Z.; Zhang, Y.; Wang, L. *J. Phys. Chem. C* **2009**, *113*, 3955.
(16) Peng, S.; Sun, S. *Angew. Chem., Int. Ed.* **2007**, *46*, 4155.
(17) Kim, D.; Park, J.; An, K.; Yang, N.-K.; Park, J.-G.; Hyeon, T. *J. Am. Chem. Soc.* **2007**, *129*, 5812.
(18) Jia, B.; Gao, L. *J. Phys. Chem. C* **2008**, *112*, 666.
(19) Hu, P.; Yu, L.; Zuo, A.; Guo, C.; Yuan, F. *J. Phys. Chem. C* **2009**, *113*, 900.
(20) Cong, Y.; Wang, G.; Xiong, M.; Huang, Y.; Hong, Z.; Wang, D.; Li, J.; Li, L. *Langmuir* **2008**, *24*, 6624.
(21) Lee, D.; Cohen, R. E.; Rubner, M. F. *Langmuir* **2007**, *23*, 123.
(22) Caruso, F.; Spasova, M.; Susha, A.; Giersig, M.; Caruso, R. A. *Chem. Mater.* **2001**, *13*, 109.
(23) Lou, X. W.; Archer, L. A.; Yang, Z. *Adv. Mater.* **2008**, *20*, 3987.
(24) Jagadeesan, D.; Mansoori, U.; Mandal, P.; Sundaresan, A.; Eswaramoorthy, M. *Angew. Chem., Int. Ed.* **2008**, *120*, 7799.
(25) Yu, D.; Sun, X.; Zou, J.; Wang, Z.; Wang, F.; Tang, K. *J. Phys. Chem. B* **2006**, *110*, 21667.
(26) Cao, S. W.; Zhu, Y.-J.; Ma, M.-Y.; Li, L.; Zhang, L. *J. Phys. Chem. C* **2008**, *112*, 1851.
(27) Wang, Y.; Angelatos, A. S.; Dunstan, D. E.; Caruso, F. *Macromolecules* **2007**, *40*, 7594.
(28) Angelatos, A. S.; Wang, Y.; Caruso, F. *Langmuir* **2008**, *24*, 4224.
(29) Bagalkot, V.; Zhang, L.; Levy-Nissenbaum, E.; Jon, S.; Kantoff, P. W.; Langer, R.; Farokhzad, O. C. *Nano Lett.* **2007**, *7*, 3065.
(30) Park, H.; Yang, J.; Seo, S.; Kim, K.; Suh, J.; Kim, D.; Haam, S.; Yoo, K. *Small* **2008**, *4*, 192.
(31) Yu, M.; Jeong, Y.; Park, J.; Park, S.; Kim, J.; Min, J.; Kim, K.; Jon, S. *Angew. Chem., Int. Ed.* **2008**, *47*, 5362.
(32) Wang, Y.; Caruso, F. *Chem. Mater.* **2005**, *17*, 953.

(33) Latham, A. H.; Wilson, M. J.; Schiffer, P.; Williams, M. E. *J. Am. Chem. Soc.* **2006**, *128*, 12632.
(34) Narayanaswamy, A.; Xu, H.; Pradhan, N.; Peng, X. *Angew. Chem., Int. Ed.* **2006**, *45*, 5361.
(35) Descostes, M.; Mercier, F.; Thromat, N.; Beaucaire, C.; Gautier-Soyer, M. *Appl. Surf. Sci.* **2000**, *165*, 288.
(36) Laurent, S.; Forge, D.; Port, M.; Roch, A.; Robic, C.; Vander Elst, L.; Muller, R. N. *Chem. Rev.* **2008**, *108*, 2064.
(37) Lou, X. W.; Wang, Y.; Yuan, C.; Lee, L.; Archer, L. A. *Adv. Mater.* **2006**, *18*, 2325.
(38) Karmakar, S.; Chakravorty, A. *Inorg. Chem.* **1996**, *35*, 1935.
(39) Narayanaswamy, A.; Xu, H.; Pradhan, N.; Kim, M.; Peng, X. *J. Am. Chem. Soc.* **2007**, *129*, 10937.
(40) Chen, Y.; Johnson, E.; Peng, X. *J. Am. Chem. Soc.* **2007**, *129*, 10937.
(41) Zhu, Y.; Shi, J.; Shen, W.; Dong, X.; Feng, J.; Ruan, M.; Li, Y. *Angew. Chem., Int. Ed.* **2005**, *117*, 5213.

JP907296N